TOWARDS NANO-G SENSING FOR HIGH PRECISION ORBITAL MANOEUVRES

A.K. Dokoupil[(1)], M.G. Beker [(1)], T.-J. Peters [(1)], H.L.M. Heeres[(1)], A. Bertolini [(2)]

[(1)] Innoseis Sensor Technologies, Science Park 105, 1098 XG, Amsterdam, The Netherlands, +3120 592 2063, info@innoseistech.com
[(2)] National Institute for Subatomic Physics Nikhef, Science Park 105 1098XG Amsterdam, The Netherlands, +3120592 2000, info@nikhef.nl

ABSTRACT

For autonomous positioning and navigation, high accuracy inertial sensor data is needed. Low-cost micro-electrical mechanical systems (MEMS)-based inertial measurement units (IMUs) available today do not provide the required level of accuracy. We present a novel MEMS accelerometer that provides acceleration data with ultra-low noise levels. This increased sensitivity is enabled by patented anti-spring technology, by means of a proof-mass suspended by leaf springs that can be pre-loaded. Using this on-chip anti-spring mechanism, low stiffness, and corresponding high sensitivity, can be combined with micro-scale devices. The stiffness reduction is independent of proof-mass position, preserves the linear properties of the mechanics and, due to its purely mechanical realization, consumes no additional power. Equivalent acceleration noise levels below 20 ng/√Hz have been demonstrated in a 50 Hz bandwidth, using a closed loop capacitive read-out. Stability measurements conducted at a low noise environment show target bias stabilities below 0.1 μg are within reach. The implications of such a sensor on satellite positioning is demonstrated by simulations on low-thrust orbital manoeuvrers. This reveals the potential to operate satellites completely autonomously, without the need to ground based positioning systems.

1 INTRODUCTION

Inertial navigation is a widely used approach to autonomous positioning and navigation. When accurate enough, it allows (autonomous) vehicles or spacecraft to stay on track or maintain orbit autonomously without the need to ground based systems. The challenge with inertial navigation is that small sensor inaccuracies quickly result into large positional errors due to integration over time. Therefore, performance requirements are stringent and extremely difficult to achieve in a compact and affordable form factor. Today's small and low-cost MEMS-based IMUs typically can only navigate standalone for tens of seconds before accumulated errors exceed acceptable margins of error. As a result, most precision navigation applications found in automotive and aerospace applications require the use of large, expensive and high-power sensor units. Furthermore, satellite positioning often requires ground based ranging systems, which are expensive and time consuming. Many applications forgo the ease of autonomy for lack of a solution with a small enough footprint. in terms of size as well as cost.

The large market gap between high-performance accelerometers and low-cost MEMS devices was the impetus to integrate the proven performance of anti-spring technology into a chip-scale silicon platform. This accelerometer concept arose during fundamental research into gravitational wave detectors at the National Institute for Subatomic Physics, Nikhef. Here, anti-spring technology for

large scale isolation and sensing apparatus was successfully miniaturised into the microscopic domain of MEMS devices. The latest prototypes of the accelerometer have noise levels below 20 ng/√Hz and a measurement range up to 0.5 g. The patented anti-spring technology allows the accelerometers to be significantly more sensitive while maintaining low power consumption. Moreover, this purely mechanical invention is cost effective, since it relies on conventional production methods.
The aim within the aerospace segment is to significantly improve the navigational capabilities of spacecraft and reduce the need to use external systems to compensate for errors with respect to orbit determination. Orbit maintenance in constellations will benefit as well, as manoeuvres can be performed more accurately. Reduced propellant consumption will make onboard resources last longer, resulting in extended operational lifetime and a more cost-effective deployment.
We present the latest developments of an ultra-sensitive accelerometer. The accelerometer system is introduced first. The performance of the sensor is presented in the sensor characterization chapter. Finally, simulations on low-thrust orbital manoeuvrers are described.

2 ACCELEROMETER SYSTEM

The different elements of our accelerometer system will be presented in more detail in this section. First, the MEMS device will be presented. After introducing the concept of geometric anti-spring technology in MEMS, the electronics readout is described.

2.1 MEMS DEVICE

The working principle of our MEMS accelerometer is based on a mass-spring system. This mechanical system can be used to measure acceleration as follows; if the frame accelerates, the inertia of the mass causes the mass to displace less than the frame. As a result, the deflection of the spring(s) will change. This change in deflection is proportional to the applied acceleration and can be used to sense the acceleration of the frame.
Within the MEMS chip, displacement of the proof-mass is measured capacitively, using arrays of finger pairs as parallel plate capacitors. Geometric anti-spring (GAS) technology enables the springs suspending the proof mass to have a very low stiffness [1].

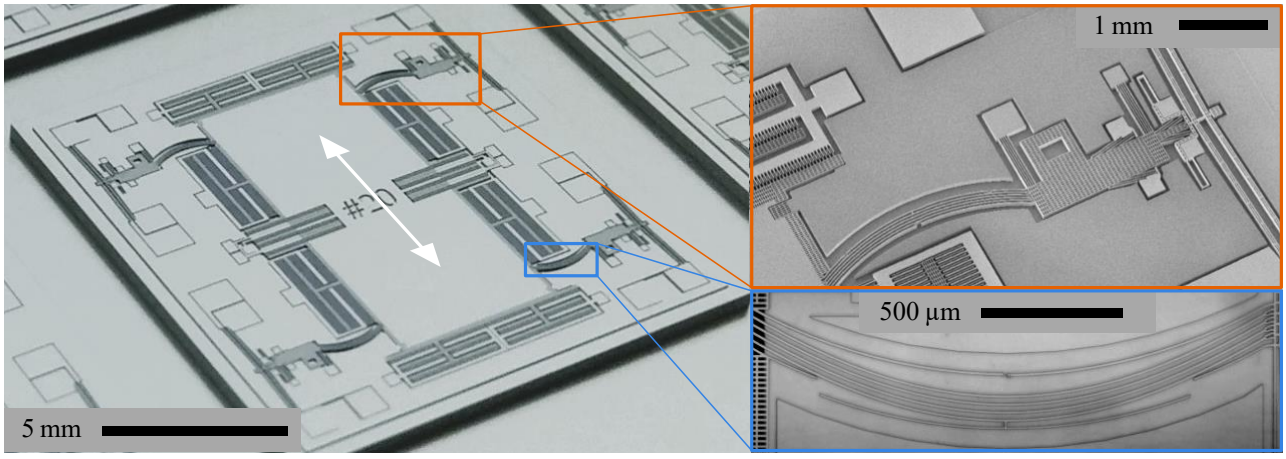

Figure 1. Microscopic image of a prototype MEMS accelerometer. The measurement axis is indicated by the white double-headed arrow. The insets on the right provide close-up views. Top: the compression system, used to pre-load a single set of springs. Bottom: a pre-loaded spring set.

2.2 ANTI-SPRING TECHNOLOGY

The concept of GAS suspension technology originates from the gravitational wave detector community. Originally, it is used at the macro scale to lower the resonance frequency of large seismic isolation filters [2]. Inspired by this macro anti-spring effect, stiffness reduction is achieved in the MEMS accelerometer by a preloading mechanism in combination with arc-shaped prismatic beam springs.

The anti-spring effect is illustrated in Figure 2. A proof mass is suspended by a total of four springs: two suspension springs parallel to and two springs perpendicular to the measurement axis. The anti-spring effect is achieved by pre-loading the two springs that are perpendicular to the measurement axis. The pre-loaded springs exert a static compression force, F_c, on the proof mass. Displacement of the proof mass along the measurement axis will result in a force $F_{cy} = -2F_c \cdot \Delta y / L_c$. This force cancels part of the restoring force exerted by the suspension springs, $F_k = k_y \cdot \Delta y$, and effectively lowers the total stiffness over the measurement axis. Adjusting F_c provides control over the stiffness in the sensing direction. It must be noted that the separate springs parallel to the sensing direction are drawn for illustrative purposes, and they are not necessarily physically separated from the springs which are pre-loaded.

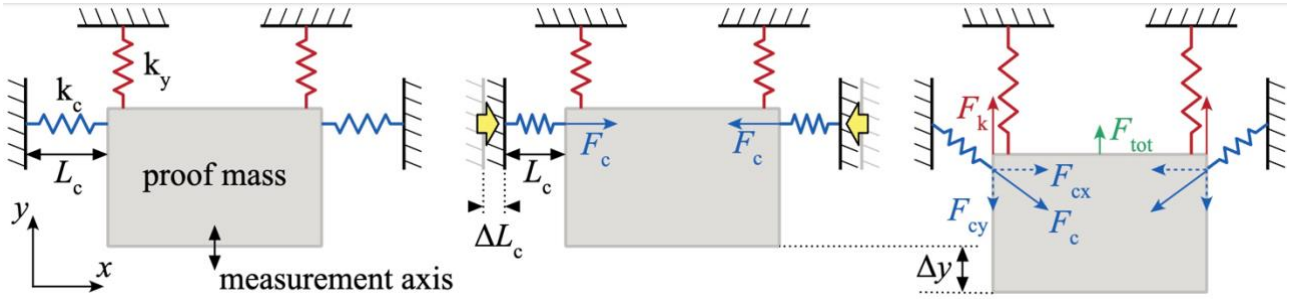

Figure 2. Conceptual illustration of the anti-spring effect. Left: system before pre-loading. Middle: proof-mass in equilibrium position with lateral pre-load F_c. Right: proof-mass in displaced state, where F_{cy} cancels most of F_k

2.3 ELECTRONICS READOUT

A dedicated electronic circuit was developed for the readout and control of the MEMS accelerometer. This circuit uses the signal from the sensing combs as input and provides feedback using actuation combs, aiming to keep the proof mass in its centered position. The electronic circuit is presented schematically as a block diagram in Figure **3**.

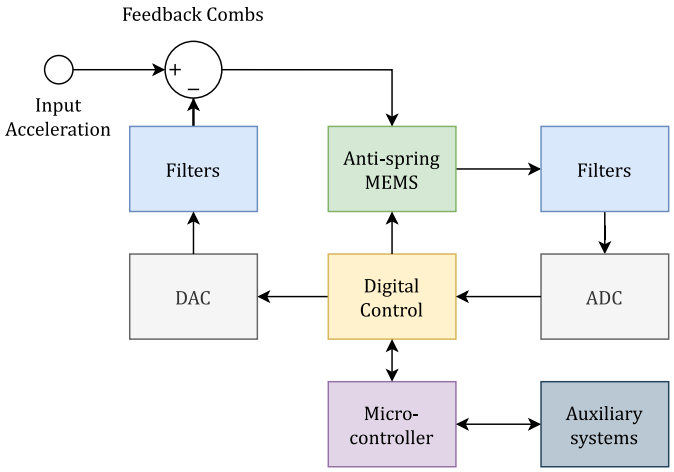

Figure 3. Schematic of the MEMS accelerometer readout and control circuit

To measure the position of the sensor proof-mass, a discrete component capacitive half-bridge readout is used. A differential sine wave is applied across the two MEMS sensing capacitors. An imbalance between the sensing capacitors due to proof-mass motion will cause a net current at the MEMS output. This signal is passed through filters before being converted into a digital signal with amplitude proportional to the difference in capacitance. A synchronous demodulator and a low-pass filter provide an output signal proportional to the proof-mass position. A digital PID controller generates a feedback signal to the MEMS actuators that keep the proof-mass in its equilibrium position. The controller output is decimated and represents the acceleration signal. The electronics include auxiliary systems such as temperature sensors, timing synchronization, data storage or communication protocols.

3 SENSOR CHARACTERIZATION

The preliminary performance of the MEMS accelerometer is evaluated using various measurement techniques. Relevant metrics concern sensitivity, stability, sensor noise, and temperature sensitivity.

3.1 Acceleration noise measurements

It is challenging to measure the noise floor of a highly sensitive accelerometer – due to its sensitivity it always measures some ambient disturbance. One solution is to use specialized vibration isolation equipment, another is to place the accelerometer in an environment with limited background vibration. For the latter solution, measurements were done at the 'Heimansgroeve', the underground seismic observatory of the Royal Netherlands Meteorological Institute (KNMI). Within the Netherlands this is known to be the most seismically quiet location. Synchronization of the acquisition between MEMS sensors was done using an external, GPS disciplined, oscillator. Three Trillium compact T120s seismometers were installed as reference sensors. Their signals were digitized using Innoseis Tremornet 2 autonomous seismic recording units, which were also synchronized using internal GPS referenced clocks.

The power spectral density of the MEMS data from a 48-hour period at the Heimansgroeve is shown in Figure **4**. The data from the reference Trillium 120s seismometer is also shown. It is evident that seismic background noise at this location is low, however, not low enough to directly measure the MEMS noise across the full bandwidth. Correlation techniques were used to determine the noise level more accurately [3]. From this data we can already estimate that the velocity random walk (white noise) is roughly 20 ng/√Hz and flicker noise of 28 ng.

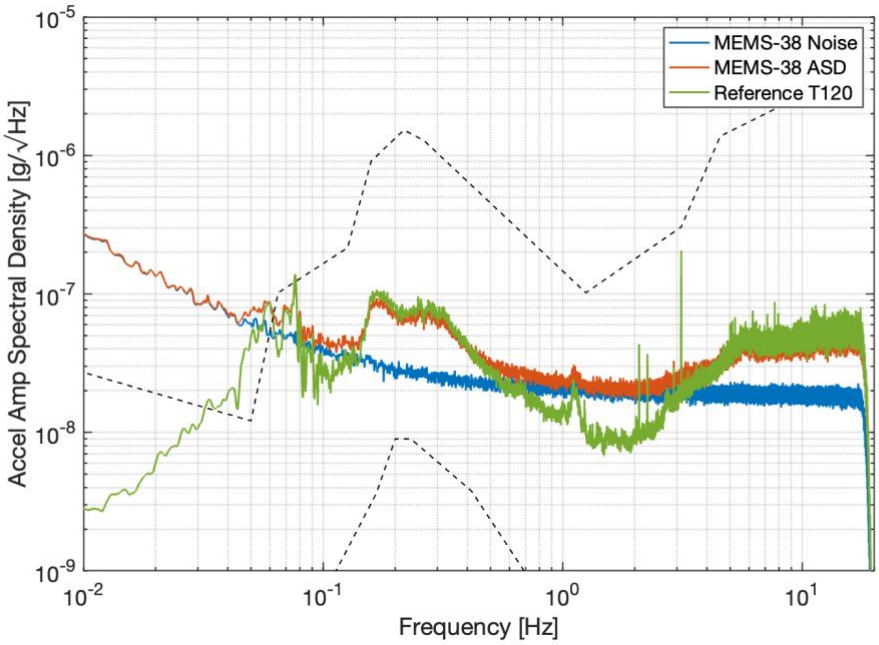

Figure 4. Amplitude power spectral density of 24 hours of continuous data. The red curve is the MEMS sensor output, the green curve the Trillium 120s reference seismometer and the blue curve the MEMS sensor noise derived from three channel correlation analysis. The thin dashed black lines indicate the Peterson new high and low noise models [4].

3.2 **Stability measurements**

To understand the bias stability performance, an Allan variance plot is typically used. It is a measure of the stability of the acceleration measurement over varying time intervals, τ. It can be calculated directly from the PSD values of the measured noise derived from the correlation analysis, and is shown in Figure 5. Here the target stability of 0.1 µg is also plotted, and it is evident that this criterion is achieved for all but the longer time intervals depending on the device and the measurement period.

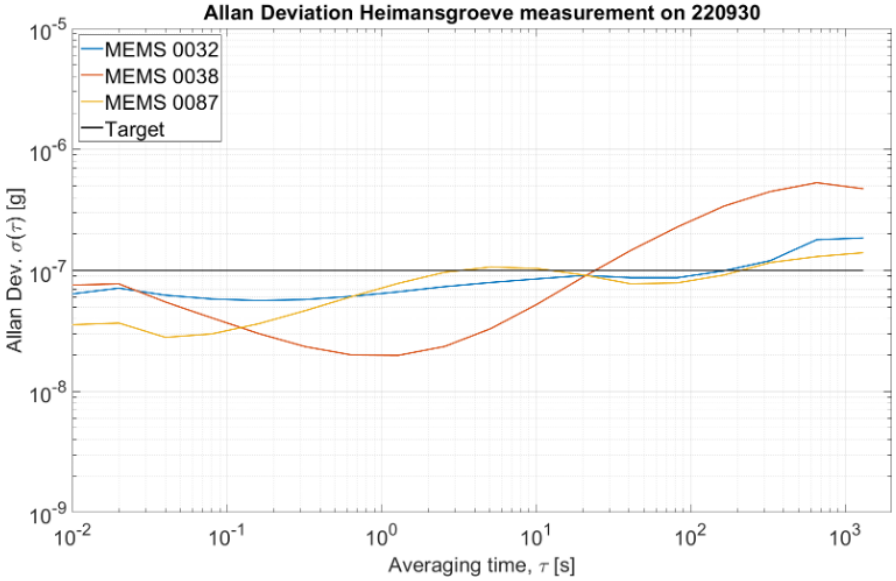

Figure 5. Allan variance of the MEMS accelerometers at the Heimansgroeve measurements. The target of 0.1 µm is indicated by the black curve

4 ORBIT KEEPING SIMULATION

A campaign of simulations was set out to determine the relative impact of the various error terms affecting the accelerometer and the performance in a test case. The chosen test case was the direct measurement of low thrust and long duration manoeuvres on a spacecraft in geostationary orbit: 70 mN thrusters on a 1000 kg satellite were engaged for 25 minutes at a time, producing a simulated continuous acceleration of 7 µg. The accelerometer error terms analysed were bias random walk (BRW), bias instability (flicker noise), velocity random walk (VRW, or white noise), mechanical noise, bias residual, and scale factor error.

Two approaches were taken in the error term evaluation: an analytical approach, using the covariance propagation method [5], and a numerical approach with a Monte Carlo analysis. The analytical analysis offers a relatively straight forward insight into the contributions of some of the accelerometer error terms – in this case BRW, VRW and scale factor error. A comparison was made between a conventional MEMS accelerometer and the accelerometer presented here. The error contributions were modelled by their amplitude spectral densities $(A_{\mathrm{VRW}}, A_{\mathrm{BRW}}, A_{\mathrm{SFRW}})$ for the conventional and anti-spring MEMS with values $\left(\frac{100\mu g}{\sqrt{\mathrm{Hz}}}, \frac{100\mu g}{\sqrt{\mathrm{hr}}}, \frac{150\mathrm{ppm}}{\sqrt{\mathrm{hr}}}\right)$ and $\left(\frac{20\mathrm{ng}}{\sqrt{\mathrm{Hz}}}, \frac{200\mathrm{ng}}{\sqrt{\mathrm{hr}}}, \frac{100\mathrm{ppm}}{\sqrt{\mathrm{hr}}}\right)$ respectively. Simulation results for a constant thrust of 7 µg over a 50 second period are shown in Figure **6**. It is shown that from the modelled disturbances, the largest contribution to the error budget is from the bias random walk. The position error for the conventional accelerometer accumulates rapidly with the anti-spring accelerometer showing improved positioning accuracy by over three orders of magnitude.

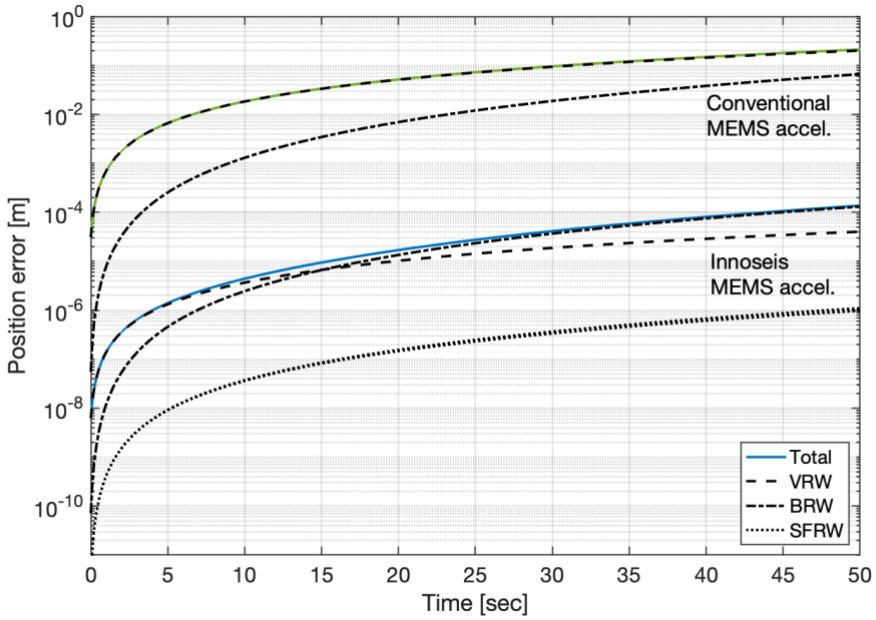

Figure 6. Covariance propagation simulation results for a conventional and an anti-spring MEMS accelerometer. The accumulated position error is calculated during a constant thrust manoeuvrer of 50 seconds.

The Monte Carlo analysis is a useful tool for comparison with analytical models and to expand the simulations to include additional noise contributions such as bias residual and instability. Comparable results are found for the analytical and Monte Carlo approaches for the bias, velocity, and scale factor random walk disturbances. The largest error term after bias compensation, was again the bias random walk. An example of the velocity error, or delta-V, during a 25-minute thrust manoeuvre from 100 Monte Carlo runs is shown in Figure **7**. From these findings it can also be concluded that in the further development of the accelerometer and its read-out electronics particular care should be taken to

reduce bias residual and bias random walk, while the requirements could be relaxed on factors that influence velocity random walk and scale factor error.

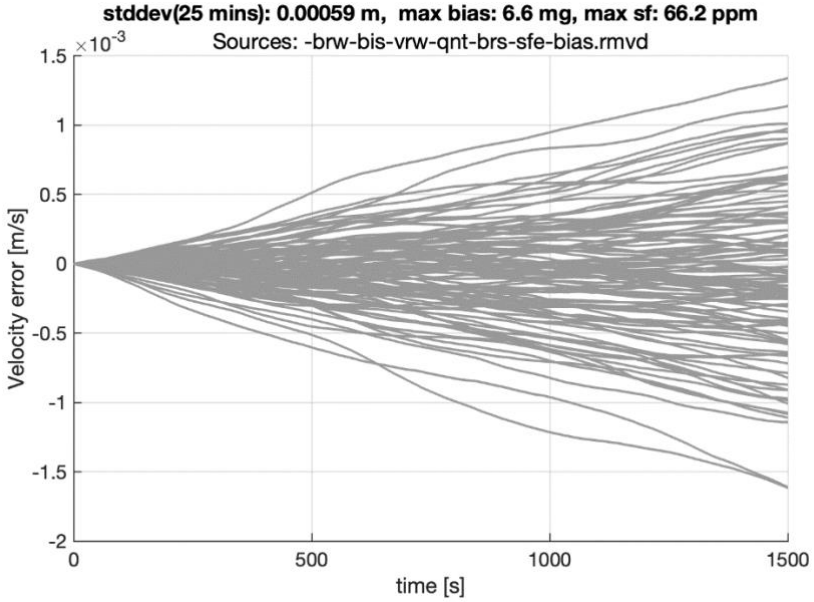

Figure 7. 100 Monte Carlo simulations with all error terms as a function of time with application of bias residual removal

Accounting for all noise terms the delta-V is shown to be less than 1%. In terms of orbit keeping for geostationary spacecraft, the 1σ delta-V error after a thrust manoeuvre is 5.9×10^{-4} m/s. Such spacecraft, using low thrust propulsion, typically make manoeuvres every second day to stay within its slot of 150 km on the geostationary arc. The typical yearly delta-V for east west manoeuvres is 3−4 m/s or only 2 cm/s per day that a manoeuvre is executed. Considering this, the accuracy of the accelerometer during the simulated manoeuvre is sufficiently accurate to achieve autonomous navigation for orbit keeping.

5 SUMMARY AND CONCLUSIONS

The work presented here highlights key aspects of a novel sensor development with application in next generation inertial navigation for satellites and other spacecraft. Characterisation and testing were a key part of the project with significant time spent on the definition of specifications. Various measurement campaigns were performed, demonstrating the preliminary performance of the MEMS devices. Measurements conducted at a low-vibration environment, showed noise levels of 20 ng/√Hz. Allan variance analysis of the same data demonstrated 0.1 µg stability over a significant measurement bandwidth. Results of bias measurements at various temperatures revealed an expected amount of temperature sensitivity. A summary of all the measured specifications is given in Table **1**. Future activities will dive deeper into the performance analysis of the accelerometers and include elements such as thermal, shock, and radiation tolerance. Results of simulations have demonstrated the added value of the improved performance. In the case of orbit maintenance of a geostationary space craft, the new sensors monitor thrust manoeuvres more precisely, allowing autonomous station keeping and reducing the need for ground-based orbit determination.

Table 1: Summary of target specifications and their preliminary measured values

Parameter	**Target / specification**	**Measured value**
Input range	0.2 – 2 g	0.2 g
Bias stability	< 0.1 μg	0.02 – 0.5 μg
Scale factor error	< 80 ppm	< 100 ppm
Velocity random walk	10 – 40 ng/√Hz	20 ng/√Hz
Bias instability (flicker)	14 – 56 ng	28 ng
Bias random walk	190 – 760 ng/√hr	750 ng/√hr
In-band noise: (0 -10 Hz)	42 – 170 ng_{rms}	125 ng_{rms}
(10 – 100 Hz)	95 – 400 ng_{rms}	190 ng_{rms}

6 REFERENCES

[1] Boom B.A., et al., *IEEE 30th International Conference on Micro Electro Mechanical Systems (MEMS)*, Las Vegas, pp. 33-36, 2017, doi: 10.1109/MEMSYS.2017.7863332.

[2] Bertolini A., et al., *Nuclear Instruments and Methods in Physics Research Section A: Accelerators, Spectrom- eters, Detectors and Associated Equipment*, vol. 435, no. 3, pp. 475 – 483, 1999.

[3] Sleeman, R., Wettum, A.H., and Trampert, J., *Bulletin of the Seismological Society of America*, Vol. 96, 258-271, 2006.

[4] Peterson, J., *U.S.G.S, Open File Report*, 93-322, 95 p, 1993.

[5] Tellinghuisen J., *The Journal of Physical Chemistry A,* Vol. 105, 15, 3917–3921, 2001.